International Journal of Scientific Engineering and Research (IJSER)
ISSN (Online): 2347-3878 (UGC Approved, Sr. No. 48096)
Index Copernicus Value (2015): 62.86 | Impact Factor (2015): 3.791

Effect of Different Inter-Electrode Distances on Order-to-Chaos-to Order Transitions in Co-Axial Electrode DC Glow Discharge

R. Kumar[1], R. Narayanan[2]

[1]Department of Applied Sciences, Meerut Institute of Engineering and Technology, Meerut-250005, India

[2]Centre for Energy Studies, Indian Institute of Technology Delhi, Hauz Khas, New Delhi-110016, India

Abstract: ***This paper attempts to understand the role of the electrode dimensions in the evolution of order-to-chaos-to-order transitions in a co-axial DC electrode discharge system, wherein the ratio of the anode-to-cathode radii is observed to determine the evolution path of the transition. Further the anode dimensions is observed to determine the discharge conductivity after the 1st negative differential resistance (NDR) region and the onset of the order-to-chaos-to-order transition is linked to the cathode dimensions.***

Keywords: DC discharge characteristics, negative differential resistance, floating potential oscillations and dynamical changes in the system

1. Introduction

Plasma discharges being a nonlinear medium, observations of associated hysteresis effects at negative differential regions (NDR) are signatures of the nonlinear dynamical evolution of the system. Such hysteresis loops are quite commonly observed near the Townsend breakdown and abnormal glow discharge regions of a planar electrode DC plasma discharge. However, there have also been observations of NDR regions in discharge [discharge current versus bias voltage] characteristics of systems such as the DP machine [1] and coaxial electrode geometry [discharge current (I_d) versus discharge voltage (V_d) characteristics] systems [2], in which the dynamical evolution of the system has been characterized using fluctuation signals [2-6] obtained from the plasma. In different systems and under different operating conditions, the fluctuation signals have been observed to undergo order-to-chaos [7] as well as chaos-to-order [8, 9] transitions. Order-to-chaos-to-order transitions [2, 10] have also been observed recently.

As reported earlier, the I_d-V_d characteristics [2, 11, 12] of the DC coaxial electrode discharges with a powered central anode have been observed to have two consecutive negative differential resistance (NDR) regions. The 1st NDR has been observed to be correlated to an upper voltage threshold whereas the 2nd NDR is seen to be linked to the discharge current [11]. The voltage drop across the 1st NDR is seen to trigger relatively large amplitude floating potential oscillations in comparison to those prior to the 1st NDR region. These oscillations, thereafter, are seen to undergo an order-to-chaos-to-order transition with increasing discharge current. As the I_d - V_d characteristic behavior seems to be linked to the polarity direction of the electrode configuration, the role of the dependence on the electrode geometry seems to be an important factor.

This paper reports the discharge characteristics and evolution of the system in co-axial electrode geometry with different inter-electrode distances, by varying the diameters of the anode/cathode.

2. Experimental Setup

The experimental setup (Fig. 1) consists of a coaxial stainless steel electrode system (≈6 cm long), with the central axial rod (diameter ≈ 0.15 cm) being the powered anode and the outer cylindrical tube (inner diameter ≈ 4.8 cm) acting as the grounded cathode. The coaxial electrode system rests on a teflon platform at a height of 16 cm from the base of the vacuum chamber (I.D. = 15.0 cm, height = 38.3 cm), in which the electrode system is enclosed. The teflon is shielded from direct contact with the plasma by using a thin mica sheet. The top end of the electrode system is open. The pumping section is at the bottom of the vacuum chamber whereas the top flange has a viewing port (quartz plate of diameter = 9 cm) for

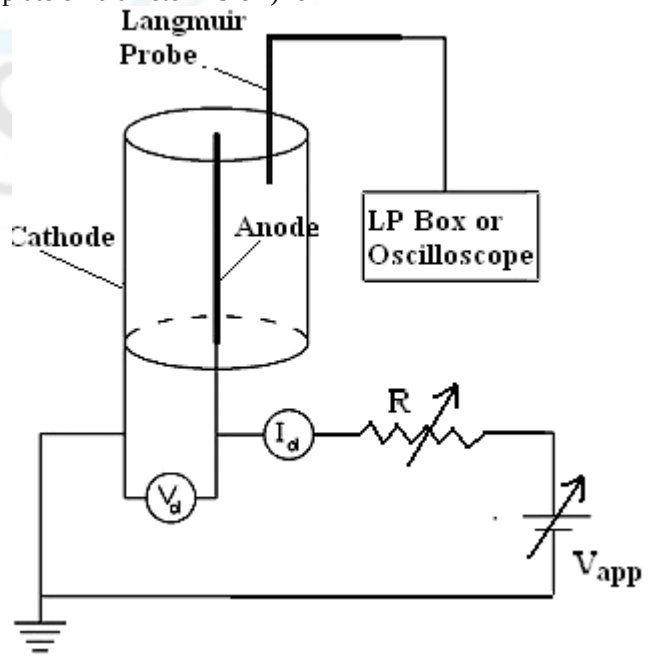

Figure 1: A schematic diagram of the electrode system and external circuit connection. The location of insertion of the Langmuir probe is also shown

carrying out spectroscopic measurements and taking plasma images. The vacuum chamber has three side ports (each of diameter r = 6 cm) at a height of 27 cm from the base of the chamber. One of the side ports is used for inserting the Langmuir probe (as shown in Fig 1) and another is used as an Argon (Ar) gas inlet port with the vacuum gauges (Micro-Pirani and capacitance manometer) mounted on the third side port. The external circuit is completed through a variable DC power supply (1 kV, 1 A), variable resistances and an ammeter.

3. Experimental Results and Discussion

In this paper, experiments have been carried out with central anode diameters of 1.5 mm and 12 mm and outer diameters of the grounded cathode being 50 mm and 70 mm, thickness of 1 mm. Experimental results from three different inter-electrode distances [viz., (1.5, 50), (1.5, 70) and (12, 70)] with an anode to cathode radii ratio of (1/33), (1/47) and (1/6) respectively are presented in this paper. The three configurations are henceforth called Set A, Set B and Set C respectively. A single Langmuir probe has been used for plasma parameter radial profile measurements at an operating pressure of 850 mTorr.

Fig. 2 shows the I_d-V_d characteristics, both for increasing and decreasing currents, for the three different inter electrode distances. The voltage threshold voltage (V_{th}) at which the 1st NDR occurs is seen to decrease with an increase in the cathode/anode diameters, with the threshold dropping from 297 V to 273 V to 250 V in Set A, B and C electrode configurations respectively. It is interesting to note that the discharge current at which the 1st NDR is triggered is the same (~3.5 mA). The dominant effect is observed when the anode rod diameter is increased. The voltage drop (ΔV_d) across the 1st NDR is seen to decrease from 53 V to 35 V to 25 V. It is further observed that the conductivity of the system after the first NDR seems to increase with change in the central anode diameter, as seen by the sustenance of the discharge at a lower discharge voltage for Set C configuration, which however, does not seem to change much for Set A and Set B.

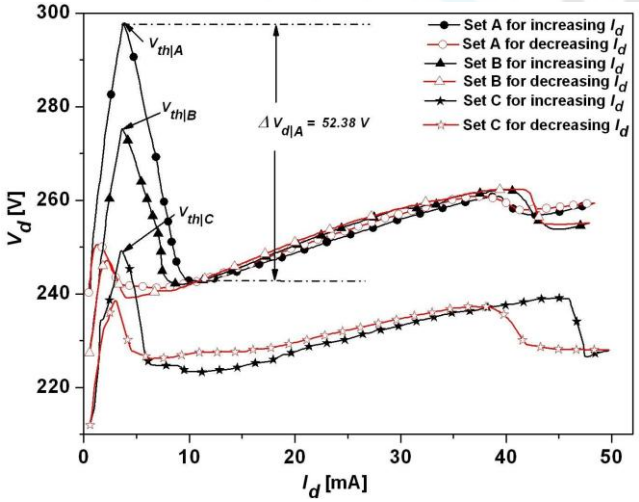

Figure 2: I_d-V_d discharge characteristics for increasing (black) and decreasing (red) I_d for different inter-electrode distances at p=850 mTorr. $V_{th|A}$, $V_{th|B}$ and $V_{th|C}$ are the threshold voltages at 1st NDR for Set A, B & C respectively. $\Delta V_d|A$ is the voltage drop across the 1st NDR for Set A.

The region between the 1st NDR and 2nd NDR is seen to undergo an order-to-chaos-to-order transition [2, 10] in the floating potential oscillations. Similar features have been observed for all the different electrode configurations reported here. However, the regions of onset of this transition and their behaviour are not same for all the configurations. Figs. 3, 4 and 5; show three representative oscillations, for each of the Sets A, B & C, depicting an order-to-chaos-to-order transition as one increases I_d. It is to be noted that oscillations at other I_d's have also been recorded but not shown here.

For Set A, it is observed that after the 1st NDR, the oscillations have an ordered behaviour from $I_d \approx$ 8.34 mA to 15.9 mA whereas the chaotic zone is from $I_d \approx$ 16.0 mA to 18.0 mA. Thereafter the oscillations remain ordered up to the maximum discharge current (46.0 mA) recorded. For Set B, the oscillations show order at $I_d \approx$ 7.10 mA, just after the 1st NDR. These remain ordered up to 8.10 mA of I_d value. The chaotic zone is observed to widen from $I_d \approx$ 8.20 mA to 28.8 mA. The oscillations at $I_d \approx$ 29.0 mA is observed to be ordered. At $I_d \approx$ 31.10 mA and $I_d \approx$ 33.0 mA, the system again becomes chaotic. At $I_d \approx$ 35.5 mA, it is ordered again. At $I_d \approx$ 37.0 mA to 42.0 mA, the system is chaotic. As the control parameter limit is reached, the system becomes ordered again (i.e. between $I_d \approx$ 42.8 mA to 45.0 mA). Thus it is seen that in this configuration, the system traverses the order-chaos-order path again and again. In Set C, the oscillations depict order in the current range $I_d \approx$ 7.10 mA to 24.5 mA whereas from $I_d \approx$ 25.0 mA to 29.0 mA, it is chaotic and thereafter at higher I_d's, the system tends to become ordered as I_d is increased to 48.0 mA.

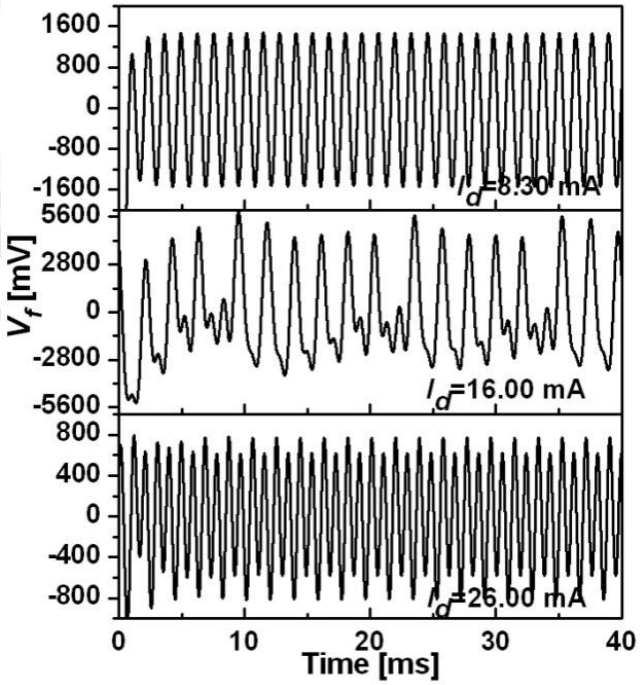

Figure 3: Floating potential oscillations for increasing discharge current for Set A at p=850 mTorr.

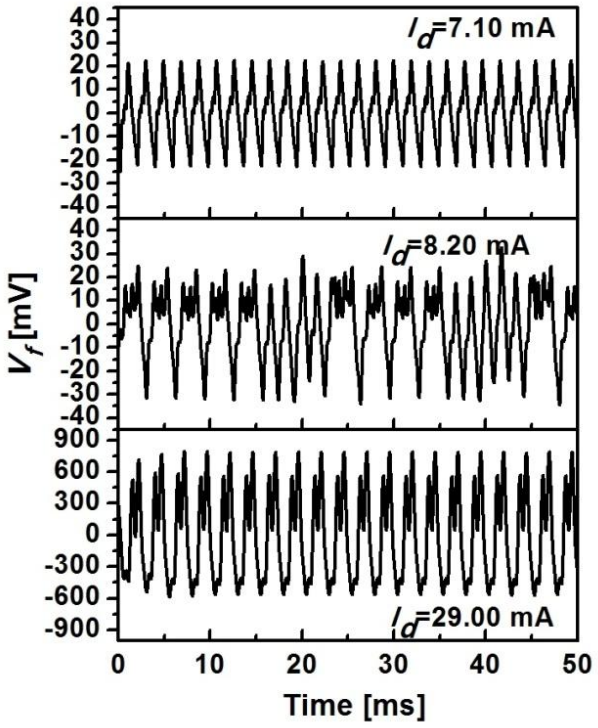

Figure 4: Floating potential oscillations for increasing discharge current for Set B at *p*=850 mTorr.

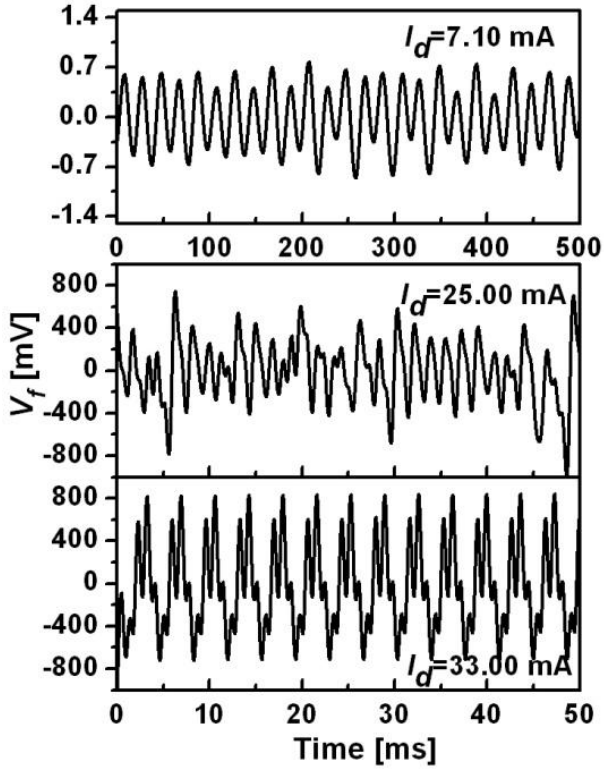

Figure 5: Floating potential oscillations for increasing discharge current for Set C at *p*=850 mTorr.

4. Characterizations of Fluctuations

The onset of the chaos-order-chaos region and it's evolution pattern seems different and thus a basic characterization of these fluctuations were carried out with respect to I_d. The amplitude bifurcation of the oscillations shown in Fig. 6 for Sets A, B and C show that the onset of the chaotic region starts at higher and higher I_d values as one shows from Set A to Set B to Set C configurations respectively. The current jump is more significant from Set A to Set B. Further, the behavior of the bifurcation diagram seems to evolve differently in the three cases, with the system tending to become ordered more slowly when the inter electrode distance is maximum (Set B).

The amplitude levels also show an interesting trend. As seen in Set B of Fig. 6, at $I_d \approx 21.3$ mA, the amplitude of oscillations suddenly increase and tends to remain in this increased level up to $I_d \approx 31.10$ mA. Thereafter at $I_d \approx 33.0$ mA, the amplitude levels of oscillations show a decreasing trend till the control parameter limit. Comparing this with Set A and Set C, one finds in these sets that the large amplitude phenomenon tends to decrease relatively faster after a certain current limit with the amplitudes remaining at lower levels (~ 20 mV). Thereafter, the amplitude decay rate is slightly slower in Set C as compared to Set A. It may be possible that one observes such reduction in amplitude levels at higher I_d in Set B also but at present the experimental set up does not have the facility to go to such high discharge currents.

In order to understand the deviation of the oscillations from the DC level, their variance has been estimated (Fig. 7) which reveals that the variance is large in the region of the chaotic regions and hence onset of maximum variance tends to shift to the right i.e. linked to the onset of the order-to-chaos-to-order transition with the largest shift being observed when the cathode diameter is changed (i.e. Set A to Set B/C) as observed in Fig. 5 also.

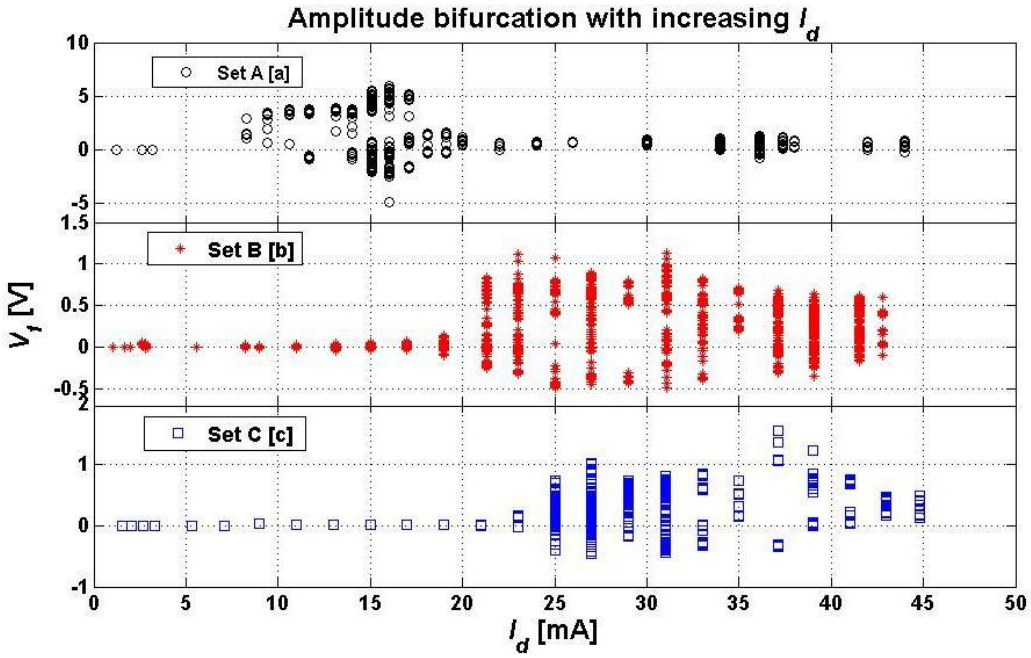

Figure 6: Amplitude bifurcation diagram from the different electrode dimensions at p= 850 mTorr: (a) Set A, (b) Set B, and (c) Set C.

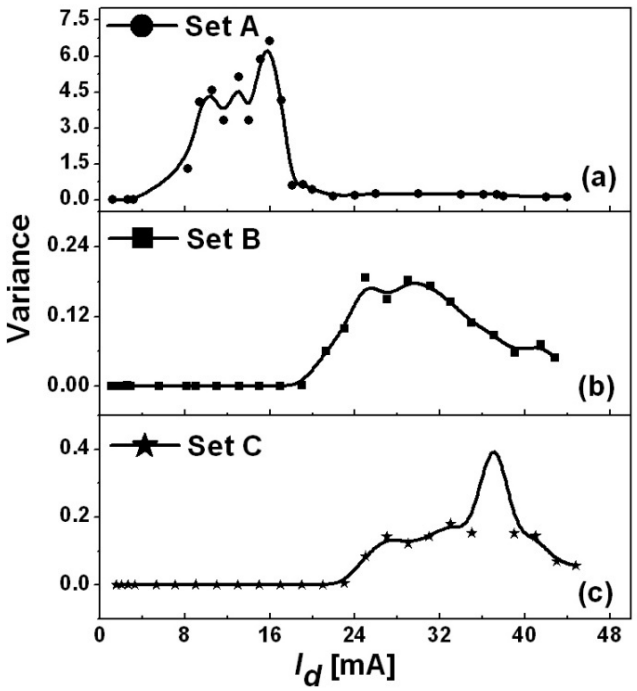

Figure 7: Variance versus I_d for the different electrode dimensions at p= 850 mTorr: (a) Set A, (b) Set B, and (c) Set C.

5. Conclusion

The changes in the onset of the 1st NDR when one characterizes Set A, Set B and Set C configuration; show that the NDR is triggered at significantly higher conductivity as the electrode surface area is increased and the system transits to a significantly higher conducting state after 1st NDR when the anode diameter is changed. However, the onset of the order-to-chaos-to-order transition seems to be governed by the cathode dimensions. Further it needs to be stated that the evolution of the order-to-chaos-to-order zone seems dependent on a critical value of the ratio of anode-to-cathode radii which needs to be investigated further.

6. Acknowledgments

Authors would like to thanks Mr. A.J. Jose Kutty for their technical support and R.K. also give thanks to Council for Scientific and Industrial Research, India for giving the scholarship during Ph.D. period.

References

[1] C. Ionita, D. G. Dimitriu, and R. W. Schrittwieser, Int. J. Mass. Spectrom. **233**, 343-354 (2004).
[2] R. Kumar, R. Narayanan and A. Prasad, Phys. Plasmas **21**, 123501 (2014).
[3] Md. Nurujjaman, R. Narayanan, and A. N. S. Iyengar, Chaos **17**, 043121 (2007).
[4] Md. Nurujjaman and A. N. S. Iyengar, Phy. Lett A **360**, 717-721 (2007).
[5] Md. Nurujjaman, R. Narayanan, and A. N. S. Iyengar, Phys. Plasmas **16**, 102307 (2009).
[6] S. Gurlui, D. G. Dimitriu, C. Ionita, and R.W. Schrittwieser, Rom. Journ. Phys. **54**, 705-710 (2009).
[7] V. Mitra , A. Sarma, M.S. Janaki, A.N. Sekar Iyenger, B. Sarma, N. Marwan, J. Kurths, P. K. Shaw, D. Saha, S. Ghosh, Chaos, Solitons & Fractals **69**, 285-293 (2014).
[8] S. Lahiri, D. Roychowdhury, and A. N. S. Iyengar, Phys. Plasmas **19**, 082313 (2012).
[9] Md. Nurujjaman and A. N. S. Iyengar, Pramana, J. Phys. **67**, 299-304 (2006).
[10] M. Agop, D. G. Dimitriu, L. Vrajitoriu, and M. Boicu, J. Phys. Soc. Jpn. **83**, 054501 (2014).
[11] R. Narayanan, R. Kumar, R. D. Tarey, A. Ganguli, Proceedings of PPPS-2013 held in San Francisco, California, USA from June16-21, 2013, Publ. IEEE & POD Publ. Curran Associates, Inc. ISBN: 978-1-4673-

5166-9, **1**, 435-438 (2014).

[12] R. Kumar, R. Narayanan, R. D. Tarey, A. Ganguli, "Hysteresis Flip Effects On the DC Plasma Discharge Characteristics Of A Co-Axial Electrode Geometry", Presented in XXXII International Conference on Phenomenon in Ionized Gases, July 26-31, 2015, Iasi, Romania.